MR quantification of cerebral ventricular volume using a semiautomated algorithm.

L A Johnson, J D Pearlman, C A Miller, T I Young and K R Thulborn

AJNR Am J Neuroradiol 1993, 14 (6) 1373-1378
http://www.ajnr.org/content/14/6/1373

MR Quantification of Cerebral Ventricular Volume Using a Semiautomated Algorithm

L. A. Johnson, J. D. Pearlman, C. A. Miller, T. I. Young, and K. R. Thulborn

PURPOSE: A semiautomated border identification algorithm, insensitive to user bias, is evaluated for accuracy and speed in the measurement of ventricular volumes from three-dimensional MR images. **METHODS:** A three-dimensional gradient-echo technique was implemented on a Signa clinical imaging system. Data from phantoms and patients were analyzed for volume using a segmentation algorithm designed with: 1) correction for partial volume averaging; 2) insensitivity to user bias; and 3) speed. Accuracy, precision, and intra- and interobserver variability were determined. **RESULTS:** Average error for phantom studies was 4% to 6%, or 1 to 2 cc across the volumes, which ranged from normal to mild hydrocephalus (<60 cc). Patient studies showed intra- and interobserver error of 2.3% and 7.8%, respectively. The correction for partial volume averaging resulted in a threefold decrease in error. Data were acquired and reconstructed within 7 minutes. Experienced radiologists required less than 15 minutes to perform each analysis. **CONCLUSIONS:** This algorithm allows accurate measurement of ventricular volumes in an efficient, minimally supervised manner.

Index terms: Brain, ventricles; Brain, volume; Brain, occipital lobe; Brain, magnetic resonance; Magnetic resonance, 3-D; Degenerative brain disease

AJNR 14:1373–1378, Nov/Dec 1993

Accurate determination of cerebral ventricular volumes can be important for the diagnosis of hydrocephalus and can provide important follow-up information in patients with intraventricular shunts. Changes in cerebrospinal fluid (CSF) ventricular volume also have been shown to have clinical significance in patients with Alzheimer disease (1–3) and benign intracranial hypertension (4). However, the majority of studies in the literature on measuring cerebral ventricular size have been conducted with computed tomography, often using linear or area measurements as indices of ventricular volume (3, 5–14). Those magnetic resonance studies which measured actual volumes were done with skip areas (15–18) with lower resolution than magnetic resonance can provide (19–22) or with long imaging or analysis times (1, 23–25) that are not practical for routine clinical applications.

The purpose of the present study was to test a semiautomated computer algorithm able to calculate cerebral ventricular volume rapidly with minimal operator input and to correct for partial volume effects.

Methods

Phantom Studies

Phantom Construction. A diagram of the phantom is shown in Figure 1. Three paraffin cylinders were constructed with volumes of 12.3 ± 0.5 mL (±1 SD, n = 5), 29.2 ± 0.2 mL (±1 SD, n = 5), and 58.6 ± 0.7 mL (±1 SD, n = 8). These volumes were determined by multiple measurements of the weight of water displaced by the phantoms; the average measurement was used as the true volume of the phantoms. These volumes approximate the range of ventricular volumes encountered in patients with normal to mildly enlarged ventricles, as reported in both the pathology and imaging literature (20, 26–29). The paraffin cylinders were suspended in water titrated with gadopentetate dimeglumine (Magnevist, Berlex Laboratories, Inc, Wayne, NJ), to obtain the same contrast ratio between the water and paraffin as that between brain

Received May 27, 1992; revision requested September 3, received November 16, and accepted November 23.

This work was supported by National Institutes of Health Grant RO1HL45176 and by the Whitaker Foundation.

All authors: Nuclear Magnetic Resonance Center, Massachusetts General Hospital, 13th St, Bldg 149, Charlestown, MA 02129. Send reprint requests to Keith R. Thulborn, MD, PhD.

AJNR 14:1373–1378, Nov/Dec 1993 0195-6108/93/1406–1373

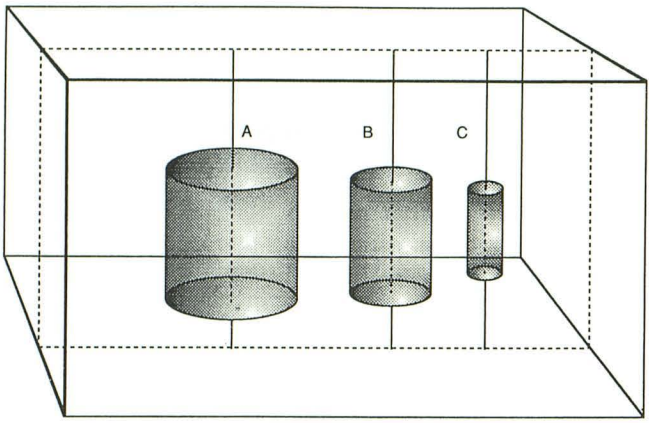

Fig. 1. Schematic representation of the paraffin-water phantom.

The paraffin cylinders (*A*, *B*, and *C*) were suspended on cotton thread to ensure that water fully surrounded them. Volumes are 58.6 (*A*), 29.2 (*B*), and 12.3 (*C*) mL measured as described in *Methods*.

parenchyma and CSF in normal brains imaged with the same gradient-echo, three-dimensional (3D) pulse sequence technique. The final concentration of gadolinium was not determined. The paraffin blocks were suspended on cotton threads in the water to ensure that water completely surrounded the cylinders. The solid paraffin cylinders avoided a physical separation between the two compartments that would artificially aid in boundary determination during image analysis.

Data Acquisition. A customized, gradient-echo 3D pulse sequence on the Signa 1.5-T imager (GE, Milwaukee, Wis; software version 3.38) was used to acquire 28 contiguous sections. The current software release (version 4.7) for Signa has a commercial equivalent of this sequence (SPGR), which has a shorter echo time (5 msec) than that available with the 3.38 software. Scan parameters were chosen for optimal brain parenchyma-to-CSF contrast and optimal signal-to-noise ratio. The parameters used were 50/9/1 (repetition time/echo time/excitations), flip angle 50°, and field of view 24 cm. Both 256 × 128 and 256 × 256 matrices were acquired for the phantom. Data sets with section thicknesses of both 3 and 5 mm were obtained on phantoms. Only 5-mm thick sections and field of view 128 × 256 were obtained on patients. Images were obtained in the coronal plane orthogonal to and at 30° to the long axis of the phantoms to provide different partial volume contributions. Patient studies were performed in the coronal plane.

Data Analysis. Images were analyzed on a Sun 4 work station (Sun Microsystems, Mountain View, Calif) using a semiautomated image segmentation package which reads data from any format and identifies borders between two contiguous compartments sampled by the operator as described below.

Before beginning the analysis, the operator selects several circular regions in the area of pure foreground (regions labeled *F* in Fig 2) to define the average intensity value of the foreground, averaged over the selected regions. This number for average intensity of the foreground is identified as pure F. To define a given boundary, such as that between CSF and brain parenchyma, the operator selects an area on each side of the desired border by placing the cursor at the appropriate positions (points *x* and *y* in Fig 2). The computer then automatically samples a circular region around each point, with a radius equal to one-third of the distance between the two selected points (*circles* labeled *X* and *Y* in Fig 2). By comparing the distribution of signal intensities in each of the two circular regions, the computer determines the border value, which results in the least number of misclassified pixels between the two populations. The border is superimposed on the displayed image, and the computer automatically classifies pixels or fractions of pixels which contribute to the total volume based on the signal intensity of each, compared with the signal intensities of the background and foreground. To provide a correction for partial volume averaging, the pure background must be sampled. This is done automatically by the algorithm by choosing a third point (labeled *b* in Fig 2) to estimate locally the background intensity. This point is located a distance half the distance between the two original points away from the previously selected point, y. A circular area with the radius equal to half the distance between the two original points is sampled (circle labeled *B* in Fig 2), generating an average signal intensity value (BSI) for the pure background region. Because circle Y is close to the desired border and contains voxels with partial voluming, it cannot substitute for circle B. The operator then confirms the region of interest (ROI) which has been outlined by the

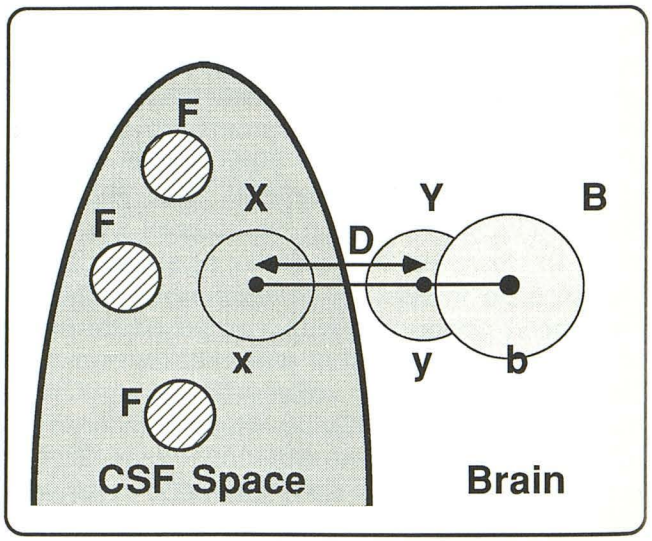

Fig. 2. Scheme for use of border-drawing algorithm as described in detail in the text.

F is the operator FSI. Points *x* and *y* are chosen by the operator to be included in the regions that will be separated by a border. The separation distance *D* between *x* and *y* determines the circular areas *X* and *Y* of radius D/3 to be sampled for each region. The third point *b* at D/2 from *y* is the center of an area B of radius D/2, used to determine the BSI. This data set determines the border, provides the partial volume correction, and calculates the volume as discussed in the text.

TABLE 1: Phantom volumes with and without correction for partial volume averaging

True Volume (ml)	Orientation	Volume (ml) Without Correction (Mean ± 1 SD)	% Error	Volume (ml) With Correction (Mean ± 1 SD)	% Error
58.6	Axial	61.5 ± 0.2	5	56.3 ± 3.2	4
29.2	Axial	30.9 ± 0.1	6	27.2 ± 1.7	7
12.3	Axial	13.0 ± 0.1	5	11.5 ± 0.7	6
Average % Error			5.3		5.7
58.6	Angle	63.8 ± 2.1	9	57.1 ± 1.5	3
29.2	Angle	33.0 ± 1.2	13	28.4 ± 1.1	3
12.3	Angle	14.2 ± 0.9	15	11.8 ± 0.4	4
Average % Error			12.3		3.9

contour map, and the volume contribution automatically determined by the computer. Using both the mean foreground signal intensity (FSI) and the mean BSI, corrections for partial volume averaging in the ROI chosen by the operator are made according to the following formula: volume * BSI − mean signal intensity of the ROI/BSI − FSI = corrected volume.

The difference in average signal intensity between the background and the ROI as a fraction of the difference in average signal intensity between the background and the foreground is multiplied by the area in pixels of the ROI to obtain a corrected volume. This accounts for partial volume averaging and is scaled by the pixel dimensions and section thickness. In summary, once the operator has selected the initial two areas of interest on either side of the desired border (points *x* and *y* in Fig 1), the border is automatically determined, and the region and corrected volume of the ROI are calculated in less than 1 sec. The computer uses the original image intensity data for calculation of the borders and the partial volume correction. The computer program also allows manual modification of any part of the border, if desired. The volumes for each region are automatically summed over the entire 3D stack to yield a final total volume after all sections have been analyzed.

Patient Studies

Six adult patients were examined with customized, gradient-echo 3D pulse sequence during a routine brain screening protocol. The average age of the patients was 50 years, with a range of 28 to 78. There were three men and three women. Two patients had a diagnosis of ventriculomegaly associated with cerebral atrophy: one had nonspecific subarachnoid enlargement with normal ventricles, one had an area of focal gliosis with normal ventricles, and two patients had normal brain MR examinations. Informed consent was obtained from all participants.

Data acquisition and analysis were performed using the techniques outlined for the phantoms. To determine the average signal intensity representing pure foreground value of CSF, ROIs were sampled by the operator from several coronal images of the lateral ventricles at their widest diameter.

Results

Phantom Studies

Results of phantom studies both with and without correction for partial volume averaging are shown in Table 1. The mean error with the partial volume averaging correction was 2 mL for the axial scans and 1 mL for the 30° angle scans. The volumes from axial images, taken in a plane perpendicular to the long axis of the phantoms, do not show a significant difference before and after partial volume correction (5.3% versus 5.7%). Presumably this is because there is very little partial volume averaging in the axial images of the phantoms. One would expect only a small amount of volume averaging in the pixels at the edges of the phantom border, and in this particular phantom the end section volume averaging was minimal because the phantom length of 6 cm allowed the acquisition of 12 5-mm sections with minimal volume averaging at the ends. However, in the 30° angle images, in which partial volume averaging effects are larger because of the oblique angle, the reduction in error when using the partial volume correction was significant and represented a threefold decrease in the average error (from 12.3% to 3.9%).

Although the volumes obtained without the partial volume corrections were higher than the true volumes (Table 1, column 3), the volumes obtained with the partial volume corrections were slightly lower (Table 1, column 5). In the phantoms with high-contrast borders, Gibbs ringing artifact along the borders resulted in lower calculated volumes because of overestimation of the true signal intensity value of the inner region. Because of the sharper borders and more severe ringing artifact in the axial phantoms, this artifact contributed to the higher percentage error of axial images than the 30° angle images.

TABLE 2: The effect of voxel size on the percent error of phantom volume measurements

ST[a] (mm)	Matrix Size	Voxel Size (mm^3)	Time[b] (min)	Large[c] Phantom	% Error	Medium[d] Phantom	% Error	Small[e] Phantom	% Error
5	256 × 128	8.79	6:35	57.3 ± 1.9	2.3	29.0 ± 0.5	0.5	12.0 ± 0.3	2.3
3	256 × 128	5.27	12:45	57.8 ± 1.6	1.4	29.6 ± 0.5	1.3	12.5 ± 0.3	1.4
5	256 × 256	4.39	10:55	59.0 ± 0.4	0.1	28.8 ± 1.2	1.3	11.3 ± 0.6	5.3
3	256 × 256	2.64	22:05	58.6 ± 0.1	<0.1	29.3 ± 0.1	0.5	12.3 ± 0.4	<0.1

Note.—Each set of images was analyzed three times by a single individual.

[a] Section thickness.

[b] Time represents the total data acquisition time and image reconstruction time.

[c] Volume = 58.6 ml.

[d] Volume = 29.2 ml.

[e] Volume = 2.3 ml.

The time required for computational analysis of the phantoms was approximately 2 seconds per section, with a total operator time, including review and selection of pure foreground and points x,y for each of 28 sections, of less than 10 minutes.

To calculate interobserver variability, results were compared between two observers. There was no significant difference in the results ($P > .05$). To test the effect of varying the voxel size on measurement errors of the phantom volumes, images were taken at a 30° angle with four different voxel sizes. The partial volume averaging correction was used. Five- and 3-mm sections were taken with both 256 × 128 and 256 × 256 matrices. The results are shown in Table 2.

Although the percent error is lower for the smaller voxel sizes, application of the Student *t* test shows that there is no significant difference between the calculated volumes when using different voxel sizes and partial volume correction ($P > .05$). However, although the calculated volumes are not significantly different, there is a substantial increase in the time of acquisition and reconstruction for the smaller voxel sizes; 6 minutes and 35 seconds for the largest voxels, compared with 22 minutes and 5 seconds for the smallest voxel.

Clinical Studies

Imaging was performed in the coronal plane because of its perpendicular orientation to the long axis of the lateral ventricles, which comprise the largest portion of the cerebral ventricular system. For a fixed section thickness, less section-to-section contour variation is seen in the lateral ventricles using the coronal plane as compared with the variation seen in the axial and sagittal planes.

TABLE 3: Intraobserver coefficient of variation

Ventricular Volumes	1st Analysis	2nd Analysis	3rd Analysis	Coefficient of Variation (%)
Right lateral	21.3	23.2	22.7	4.4
Left lateral	21.8	20.1	21.5	4.3
Third	1.8	1.6	2.6	2.7
Fourth	1.5	2.1	1.7	1.7
Total	46.4	47.0	48.5	2.3

TABLE 4: Interobserver coefficient of variation

Patient	Clinical Diagnosis	Ventricular Volume (Mean ± 1 SD)	Coefficient of Variation (%)
1	Normal	6.4 ± 0.6	9.8
2	Focal gliosis/normal ventricles	8.4 ± 0.8	9.6
3	Increased extraventricular CSF/normal ventricles	9.2 ± 1.3	14.1
4	Normal	25.4 ± 1.9	7.3
5	Cerebral Atrophy/ventriculomegaly	46.5 ± 0.4	0.9
6	Cerebral Atrophy/ventriculomegaly	62.3 ± 3.2	5.1
			Average 7.8

In the calculation of CSF ventricular volume for six patients, the intraobserver coefficient of variation determined from three calculations performed at separate points in time on one patient was 2.3% (Table 3), whereas the interobserver variation determined from examination of six patient scans by three experienced observers was 7.8% (Table 4). Although the number of this preliminary study is small, it is clear that for patients with the highest ventricular volumes (≥25 mL), which could be expected in hydrocephalus, the error is even lower (4%) than when the patients with normal ventricular volumes are included.

For a brain study, the computational analysis time is approximately 15 seconds per section,

requiring an experienced operator a total of 15 minutes to analyze an entire brain with ventricles covering 18 sections. This total time includes loading the program, reading in the images, sampling the pure foreground, and selecting x and y points for the ventricular border for each section and confirming the computer-selected ROI.

Discussion

The volumetric study of phantoms demonstrates that volume averaging contributes significantly to error when using a thresholding technique, and that this error can be dramatically improved when correction is made for partial volume averaging. Phantom studies also confirm that it is reasonable to use larger voxel sizes for cerebral ventricular volume determination, especially when clinical imaging time is limited.

The range of cerebral ventricular volumes determined from our patient studies is consistent with published values (20, 26–29). Because the 3D volume technique covers the entire ventricular system, precise alignment of the patient in the scanner from examination to examination is not required in order to compare results of ventricular volume analysis over time. We note that Figure 3 shows segmentation of the brain as the algorithm finds all tissue and CSF borders. Only the ventricles are selected in these studies. Brain volume can be measured in the same way as ventricular volume with this algorithm, and such applications will be presented elsewhere. Separation of gray and white matter also can be achieved with this algorithm, but the acquired data must be optimized for gray and white matter contrast.

The errors in data acquisition are as follows. Gibbs ringing artifact, resulting from the contrast between the water doped with gadolinium and the paraffin, is more pronounced in the axial images than in those oriented at a 30° angle to the long axis of the phantoms due to the higher contrast borders. A multisection contiguous 2D acquisition will have errors associated with the shape of the section profile, which is less important in a 3D acquisition. The difficulty in ensuring that identical sections, necessary for 2D imaging, are acquired for each study is obviated by 3D imaging. Magnetic susceptibility is another source of error, especially around air-tissue interfaces. This error is reduced with use of the short echo time of 9. Patient motion is also a source of error. The data acquisition time of less than 4 minutes minimizes voluntary patient motion. Motion of the CSF is greatest in the fourth ventricle and the aqueduct, which appear in only a few sections in the coronal orientation and represent ventricles that do not contain a large portion of the total CSF ventricular volume (Table 3).

Sources of error in data analysis include potential inaccuracy of the border determined by the algorithm. Errors arising from the choice of regions x and y (Fig 1) by the operator were found to be 1% to 2% when tested in phantoms. Other sources of error included variations in the sampling regions chosen by the algorithm to determine background brain intensity (the region labeled *B*, based on the choice of x and y in Fig 1), variations in the regions chosen to represent pure CSF (regions labeled *F* in Fig 1), and manually drawn variations in the border, chosen when the automatically drawn borders need closure in order to outline a ventricular region accurately. This last error can occur around the third ventricle

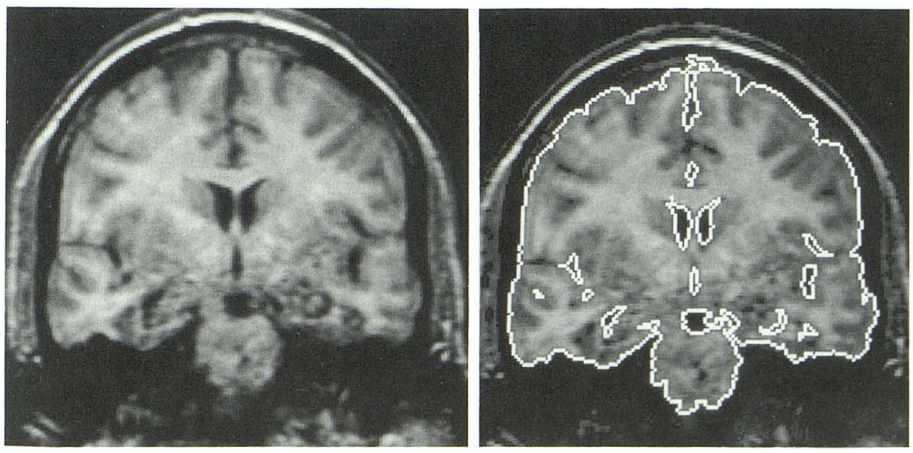

Fig. 3. A selected coronal image (*A*) from a 3D set of a human brain obtained using a customized, gradient-echo 3D pulse sequence (equivalent to the commercial SPGR sequence available from GE in the Signa version 4.7 software but with a longer minimum echo time) and the same image (*B*) segmented for ventricular volume measurement. Only the regions containing CSF are selected for the ventricular volume measurement once the border is drawn, although the brain is also outlined.

because of poor contrast between third ventricular CSF and quadrigeminal plate cisterns. These errors are all assessed by the intra- and interobserver variations calculated from the analysis of patient studies and are of an acceptable magnitude (coefficient of variation 2.3% and 7.8%, respectively, as shown in Tables 3 and 4).

Measurement of ventricular volume can be made accurately and rapidly with the described algorithm with minimal supervision.

References

1. Rusinek H, de Leon MJ, George AE, et al. Alzheimer disease: measuring loss of cerebral gray matter with MR imaging. *Radiology* 1991;178:109–114
2. George AE, de Leon MJ, Rosenbloom S, et al. Ventricular volume and cognitive deficit: a computed tomographic study. *Radiology* 1983;149:493–498
3. de Leon MJ, George AE, Reisberg B, et al. Alzheimer's disease: longitudinal CT studies of ventricular change. *AJNR: Am J Neuroradiol* 1989;10:371–376
4. Reid AC, Teasdale GM, Matheson MS, Teasdale EM. Serial ventricular volume measurements: further insights into the aetiology and pathogenesis of benign intracranial hypertension. *J Neurol Neurosurg Psychiatry* 1981;44:636–640
5. Evans WA. An encephalographic ratio for estimating the size of the cerebral ventricles. *Am J Dis Child* 1942;64:820–830
6. Hanson J, Levander B, Liliequist B. Size of the intracerebral ventricles as measured with computer tomography, encephalography, and echoventriculography. *Acta Radiol* 1975;346 (suppl):98–106
7. Hahn FJY, Rim K. Frontal ventricular dimensions on normal computed tomography. *AJR: Am J Roentgenol* 1976;126:593–596
8. Synek V, Reuben JR, Du Boulay GH. Comparing Evans' index and computerized axial tomography in assessing relationship of ventricular size to brain size. *Neurology* 1976;26:231–233
9. Gyldensted C. Measurements of the normal ventricular system and hemispheric sulci of 100 adults with computed tomography. *Neuroradiology* 1977;14:183–192
10. Haug G. Age and sex dependence of the size of normal ventricles on computed tomography. *Neuroradiology* 1977;14:201–204
11. Pfefferbaum A, Zatz LM, Jernigan TL. Computer-interactive method for quantifying cerebrospinal fluid and tissue in brain CT scans: effects of aging. *J Comput Assist Tomogr* 1986;10:571–578
12. McArdle CB, Richardson CJ, Nicholas DA, Mirfakhraee M, Hayden CK, Amparo EG. Developmental features of the neonatal brain: MR imaging. *Radiology* 1987;162:230–234
13. Gooskens RHJM, Gielen CCAM, Hanlo PW, Faber JA, Willemse J. Intracranial spaces in childhood macrocephaly: comparison of length measurements and volume calculations. *Dev Med Child Neurol* 1988;30:509–519
14. Rossi A, Stratta P, Gallucci M, Passariello R, Casacchia M. Quantification of corpus callosum and ventricles in schizophrenia with nuclear magnetic resonance imaging: a pilot study. *Am J Psychiatry* 1989;146:99–101
15. Gado M, Hughes CP, Danziger W, Chi D, Jost G, Berg L. Volumetric measurements of the cerebrospinal fluid spaces in demented subjects and controls. *Radiology* 1982;144:535–538
16. Jernigan TL, Press GA, Hesselink JR. Methods for measuring brain morphometric features on magnetic resonance images. *Arch Neurol* 1990;47:27–32
17. Cramer GD, Allen DI, DiDio LJA. Volume determinations of the encephalic ventricles with CT and MRI. *Surg Radiol Anat* 1990;12:59–64
18. Tanna NK, Kohn MI, Horwich DN, et al. Analysis of brain and cerebrospinal fluid volumes with MR imaging: impact on PET data correction for atrophy. *Radiology* 1991;178:123–130
19. Penn RD, Belanger MG, Yasnoff WA. Ventricular volume in man computed from CAT Scans. *Ann Neurol* 1978;3:216–223
20. Brassow F, Baumann K. Volume of brain ventricles in man determined by computer tomography. *Neuroradiology* 1978;16:187–189
21. Condon BR, Patterson J, Wyper D, et al. A quantitative index of ventricular and extraventricular intracranial CSF volumes using MR imaging. *J Comput Assist Tomogr* 1986;10:784–792
22. Grant R, Condon B, Lawrence A, et al. Human cranial CSF volumes measured by MRI: sex and age influences. *Magn Reson Imaging* 1987;5:465–468
23. Lim KO, Pfefferbaum A. Segmentation of MR brain images into cerebrospinal fluid spaces, white and gray matter. *J Comput Assist Tomogr* 1989;13:588–593
24. Ashtari M, Zito JL, Gold BI, Lieberman JA, Borenstein MT, Herman PG. Computerized volume measurement of brain structure. *Invest Radiol* 1990;25:798–805
25. Kohn MI, Tanna NK, Herman GT, et al. Analysis of brain and cerebrospinal fluid volumes with MR imaging. *Radiology* 1991;178:115–122
26. Last RJ, Tompsett DH. Casts of the cerebral ventricles. *Br J Surg* 1952;40:525–543
27. Schwartz M, Creasey H, Grady CL, et al. Computed tomographic analysis of brain morphometrics in 30 healthy men, aged 21 to 81 years. *Ann Neurol* 1985;17:146–157
28. Takeda S, Matsuzawa T. Age-related change in volumes of the ventricles, cisternae, and sulci: a quantitative study using computed tomography. *J Am Geriatr Soc* 1985;33:264–268
29. Caviness VS, Filipek PA, Kennedy DN. Magnetic resonance technology in human brain science: blueprint for a program based upon morphometry. *Brain Dev* 1989;1:1–13